Bahman Paygozar

TOBB University of Economics and Technology
Department of Mechanical Engineering
Ankara

Recep M. Gorguluarslan*

TOBB University of Economics and Technology
Department of Mechanical Engineering
Ankara

Bonding Additively Manufactured PLA Materials: Effects of Joint Scarf Angle and Substrate Raster Orientation

The aim of this study is to investigate the effect of the scarf angle of the bonding region and the raster orientation of 3D printed substrates for the adhesive scarf joints made of additively manufactured Polylactic acid (PLA) adherends. In the first step, single PLA specimens were 3D printed using the fused filament fabrication (FFF) process in three different raster orientations of 0º, 45º, and 90º. The joints were built with five different scarf angles. The tensile and compression tests of all the specimens were conducted to determine the failure loads for different scarf angles and raster orientations. It is found that the endured load before rupture varies measurably as a function of the raster orientation of printed substrates and scarf angle of the joint, but differently for tensile and compression loadings. An optimization was also done for the joints with substrates of 45˚ raster orientation and different scarf angles to find a suitable scarf angle, with which the joint can have an acceptable behavior (i.e. reasonable values of the failure load) under both compression and tensile loadings. Consequently, the optimal scarf angle was determined to be about 30˚.

Keywords: Adhesive scarf joint; scarf angle; raster orientation; PLA; Interlayer and Intralayer failure.

Makale Bilgisi:
Araştırma Makalesi
Gönderilme: 6 Şubat 2023
Kabul: 11 Nisan 2023

*Sorumlu Yazar: Recep M. Gorguluarslan
Email: rgorguluarslan@etu.edu.tr

DOI:
https://doi.org/10.56193/matim.1248357

Atıf şekli/How to cite: Paygozar B., Gorguluarslan R., M., Bonding Additively Manufactured PLA Materials: Effects of Joint Scarf Angle and Substrate Raster Orientation. Makina Tasarım ve İmalat Dergisi, 2023; 21(1): 33-42.

1. INTRODUCTION

Several industries have lately accepted the additive manufacturing (AM) technology with an eagerness to reduce the manufacturing costs and to raise the advantages provided through the parts produced by AM (e.g. drops in petrol usage due to reduction in the weight of cars) [1]. Potential benefits of AM technology include the fabrication of complex geometries and the reduction of products' weight, transport difficulties, and material losses, because of which AM techniques are of high interest in the automotive industry [2, 3]. AM techniques have also been suggested to be used for joining structures made from dissimilar materials such as polymers and metals [4]. Furthermore, the adhesively bonded joints have recently been used for polymeric parts fabricated by one of AM techniques called fused filament fabrication (FFF) [5].

Adhesively bonded joints are widely valued in various industries due to the advantages including uniformity of the stress distribution, tolerating large values of peel and shear strengths, low levels of stress concentration, and the negligible added weight of the joints compared to the traditional mechanical (riveting, bolting, etc.) or welded joints. Other suitable features of adhesive bonding include the applicability of adhesives in attaching a variety of materials comprising metals, composites, and 3D printed polymers [6, 7].

Among different types of adhesive bonding techniques such as the single-lap or the double-lap joints, the scarf joints are of high interest and used for industrial applications as they can eliminate some negative effects of other bonding techniques such as the bending of the substrates under loading. Moreover, the strength of scarf joints is much less affected by over stresses near the adhesive layer, when compared to single or double lap joints [8].

The use of adhesive bonding in AM industries can also enable the fabrication of parts with large dimensions, which are not possible to build by FFF machines due to their small build region (i.e. print bed of the machine) [9]. Some studies investigated bonding the additively manufactured parts with adhesives. For instance, it has been shown that modifying the adherend geometry at the adhesive bonding region and changing the raster orientation of the adherends fabricated by the FFF technique can improve the bonding of single lap joints for the Polylactic acid (PLA) material [10, 11].

Recent studies indicated that the adhesive bonding of polymeric materials fabricated by AM techniques is promising to be also used in industrial applications. It is notable that, PLA is one of the existing bio-based materials that has suitable mechanical features which makes it appropriate for automotive applications [12], where adhesive joints are broadly being used as well [13].

The main motivation of this research is that the usage of PLA material for adhesive scarf joints can be of high interest in the automotive industry due to the above-mentioned advantages. Furthermore, the existing adhesive bonding-related studies that utilized the AM techniques to fabricate polymeric adherends usually worked on single lap joints [14], which indicates that there is a need for investigating the behavior of scarf joints in the PLA adherends fabricated by AM. Two aims of the study include investigating the effects of the raster orientation and scarf angle on the failure load of scarf joints under both tension and compression loading conditions as well as optimizing the scarf angle to obtain a joint with an acceptable behavior under both compression and tensile loads. More precisely, the aim is to find a scarf angle, by which the joint can tolerate suitable amounts of loading under both loading types.

2. EXPERIMENTAL WORK

2.1 Fabrication of specimens for joint preparation

The overall configuration of the scarf joint specimen is shown in Fig. 1(a) along with the cross-sectional dimensions provided in Fig. 1(b). The adherends were manufactured by five different scarf angles (A), including 15˚, 30˚, 45˚, 60˚, and 90˚. A fused filament fabrication (FFF) 3D printer was used for manufacturing using PLA material. The longer side of each adherend has a length of 120 mm as shown in Fig. 1(a). The length of the other side is determined based on the scarf angle. In the FFF 3D printing process, the printing path of the material can have various angles between 0˚ and 90˚ called the raster orientation as shown in Fig. 1(c). In this study, the adherend specimens were printed in two different raster orientations (O), including 0˚ and 45˚, for each of the 5 scarf angles. The build plate is the xy-plane shown in Fig. 1(c). The thickness of the specimens are printed in the z-direction, i.e., the build direction. Two of the manufactured adherend specimens are illustrated in Fig. 2(a). The raster orientation of 90˚ was not considered for the adherends, since it leads to the weakest parts under tensile loading as will be shown for the results of single PLA adherends in later sections (see Fig. 4(e)).

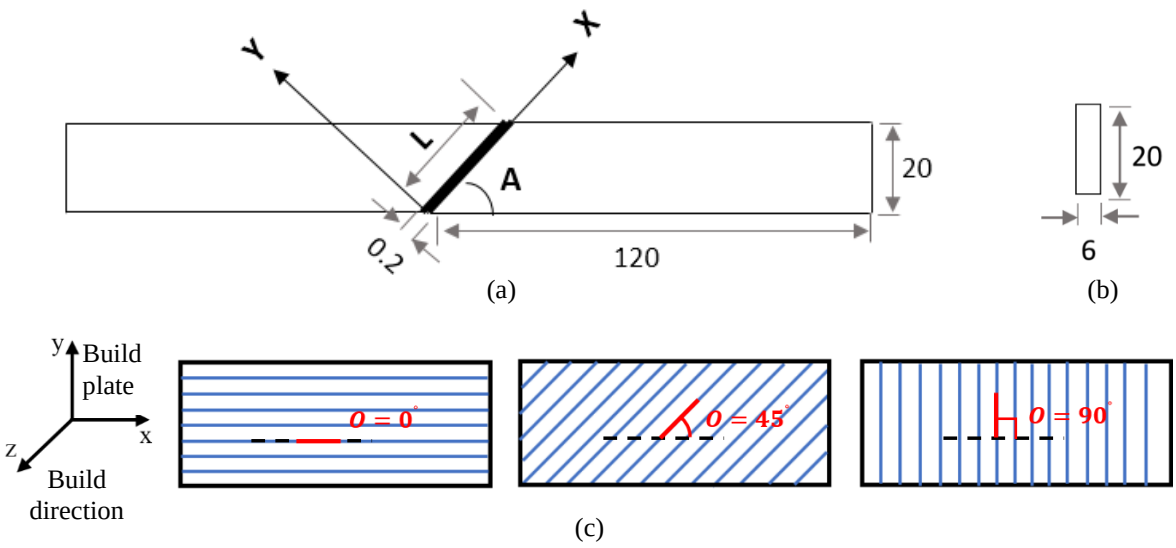

Fig. 1. Scarf joint specimen configurations (a) Top view of general configuration (b) Cross-sectional dimensions, (c) Three raster orientations of 0˚, 45˚, and 90˚ in 3D printing (from left to right, respectively). The build plate is on the xy-plane and the specimens are printed in z-direction.

The PLA adherends of the same scarf angles were attached by a thin layer of adhesive with a thickness of 0.2 mm. A structural epoxy-based adhesive, Araldite 2011 (Huntsman Advanced Materials, India), was utilized for bonding the printed PLA adherends to make the scarf joints. The surface preparation process was done according to the steps described in [11]. Both components of the adhesive were mixed in a 1:1 weight ratio [15], and in a suitable amount (50 ml). Then an appropriate amount of the mixed adhesive was applied onto the bonding surfaces of each joint. Each sample was cured in the room temperature for 24 hours under an appropriate pressure applied by a fixture, in order to obtain the maximum strength while keeping the thickness of the adhesive layer as 0.2 mm.

The prepared scarf joint samples were labeled to identify their raster orientation and scarf angle. For instance, the sample labeled as O45A30 denotes an adhesive scarf joint prepared by adherends manufactured via a raster orientation of 45˚ (O45) and a scarf angle of 30˚ (A30). Single PLA specimens were also 3D printed with the dimensions of 120×20×6 mm, in three different raster orientations of 0˚, 45˚, and 90˚ as shown in Fig. 2(b) to investigate the failure behavior of single specimens, without any bonding, under tensile and compression tests. The dimensions of the tensile and compression tests were considered to be the same as those of the adherends of the scarf joints for consistency. The labels O0C and O0T refer to a raster orientation of 0º which will be tested under compression (C) and tension (T) loadings, respectively. Similarly, O45C and O45T refer to the samples with a raster orientation of 45º used for compression and tension tests, respectively.

2.2 Tensile and compression tests

Tensile and compression tests were conducted for both single PLA specimens fabricated by the FFF process and the prepared scarf joints via a testing machine with a cross-head speed of 1mm/min. In Fig. 3, pictures of selected tests are shown to highlight different types of failure observed during the tests including interlayer, intralayer and adhesive failures. The intralayer failure refers to the damage of a PLA layer itself as in Fig. 3(a) while the interlayer failure relates to the separation of PLA layers from each other as in Fig. 3(b) and Fig. 3(c). In addition, the adhesive failure experienced in a scarf joint which reflects the damage of the adhesive layer of the joint, resulting in the debonding of the two adherends of the joint, can be observed in Fig. 3(d).

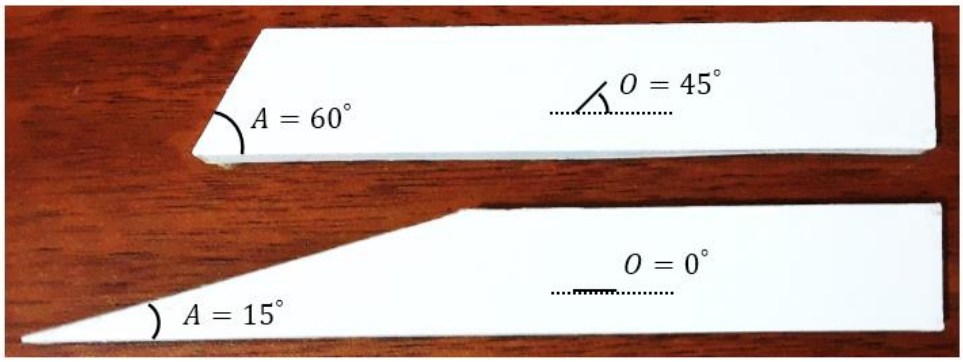

(a)

(b)

Fig. 2. Fabricated specimens (a) 3D printed PLA adherends in different scarf angles (A) and raster orientation (O), (b) the 3D printed single PLA specimens.

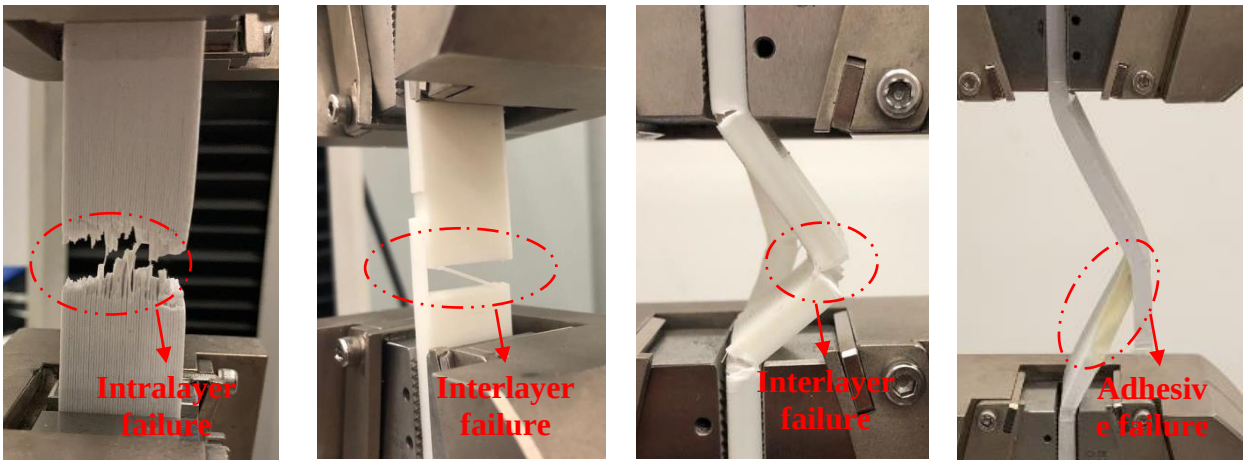

(a) (b) (c) (d)

Fig. 3. Illustration of different experiments (a) tensile test of a single PLA specimen – O0T, (b) tensile test of a single PLA specimen - O90T, (c) compression test of a single PLA specimen – O90C, and (d) compression test of the scarf joint specimen - O45A30.

3. RESULTS and DISCUSSION

3.1 Effect of raster orientation for PLA specimens

The load-displacement curves obtained from tensile and compression tests for the single PLA specimens printed in different raster orientations are illustrated in Fig. 4. The failure loads were calculated as the first peak load for each load-displacements curve. Those computed failure load values are also shown in respective graphs in Fig. 4.

It is seen in Fig. 4(a) that the load-displacement curve rises almost linearly up to a maximum level (failure load) and then goes down in several steps. This is because the raster orientation is 0˚, due to which the fracture occurs in the layers gradually without any lateral movement as shown in Fig. 3(a) (just intralayer failure). Each layer or groups of layers endure the plastic deformation and then rupture, by which loading reflection demonstrates such a step-wise pattern.

This step-wise pattern of the load curve is also the case for the compressive loading condition as shown in Fig. 4(b), in which the raster orientation is 0˚. In this case, however, the compression load leads to interlayer failure (i.e. separation of PLA layers from each other) unlike intralayer failure seen in the case of tensile loading. The failure behavior of the single PLA specimen under compression load is shown in Fig. 5(a) to highlight the difference compared to the tensile loading case shown in Fig. 3(a). In compression, buckling with out-of-plane deformation occurs as seen in Fig. 5(a). Since the bent zone in buckling is perpendicular to the PLA layers, separation is seen along the raster orientation angle of 0˚ in the middle of the buckled region in Fig. 5(a). This separation behavior in the specimen results in gradual decreases in the load-displacement curve as seen in Fig. 4(b).

When the raster orientation is 45˚, a higher displacement at peak load is observed for tensile loading as shown in Fig. 4(c). Since the raster orientation of 45˚ leads to the separation of the PLA layers, i.e., interlayer failure as well. This raster orientation causes the sample to have a failure load (4.45 kN) a bit less than that of a specimen manufactured with a raster orientation of 0˚ (5.54 kN). This is because for the raster orientation of 45˚, the separation of layers (i.e. interlayer failure) is also experienced along with the failure of the material itself (i.e. intralayer failure), and because the interlayer strength of the FFF-printed materials is lower than the strength of a layer itself (intralayer strength). This fact can be realized through the failure loads obtained from the tensile testing of the samples O0T and O90T shown in Fig 3(a) and Fig. 3(b), respectively. In particular, O90T experienced interlayer failure (i.e. failure between layers) as seen in Fig. 3(b) and had a failure load of 1.68 kN. On the other hand, O0T experienced intralayer failure as seen in Fig. 3(a), and therefore, had a much higher failure load of 5.54 kN. Figs. 4(a) and (e) indicate the load-displacement response of O0T and O90T, respectively.

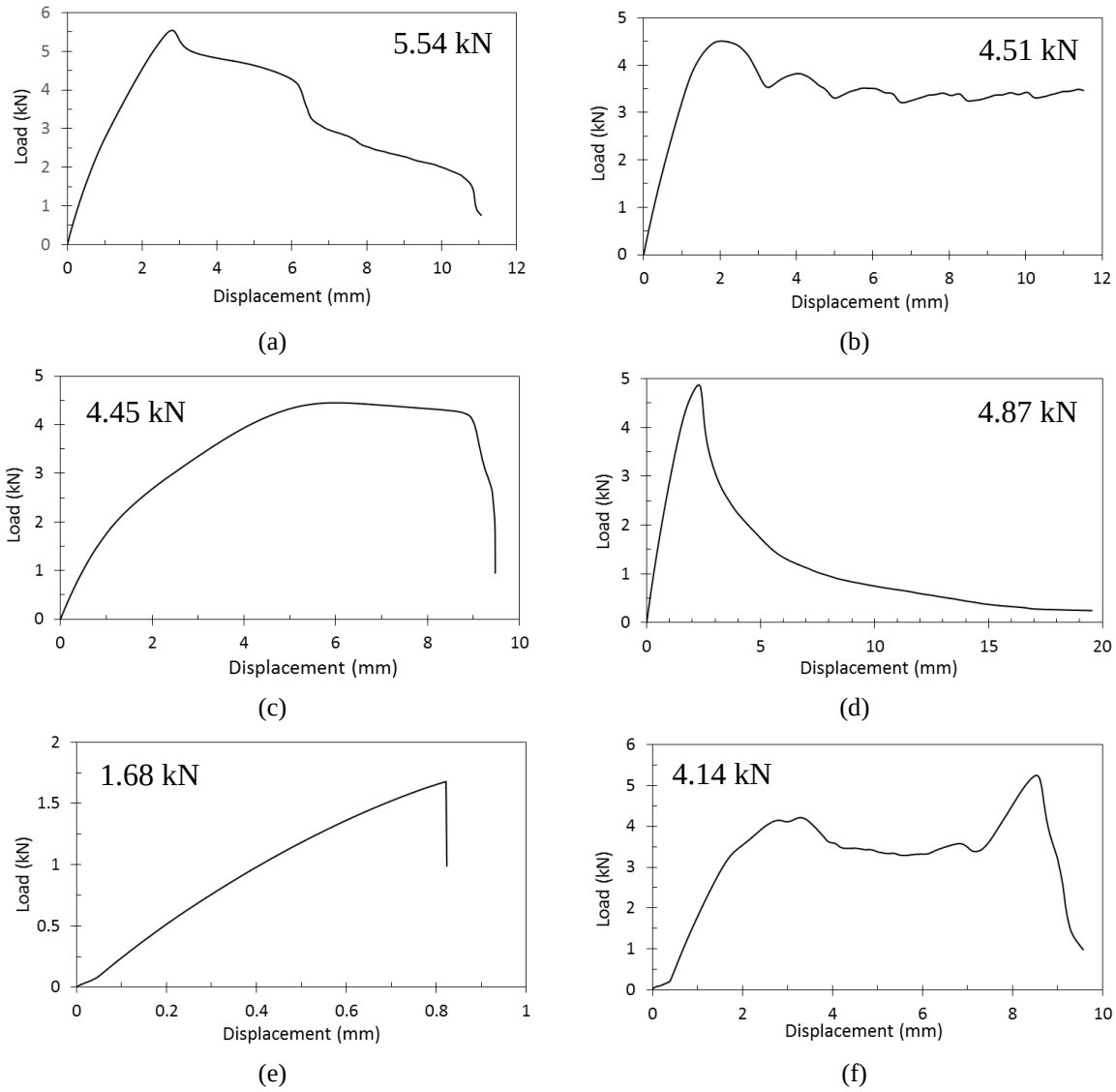

Fig.4 Load-displacement responses of single PLA specimens printed in different raster orientations; (a) O0T under tensile testing (b) O0C under compression testing, (c) O45T under tensile testing, (d) O45C under compression testing, (e) O90T under tensile testing, (f) O90C under compression testing. The failure loads are written onto the plots. In the plots related to the compression testing (b, d, and f), absolute values are given.

On the contrary, the scenario is fully different for the compression test results of the same specimens, i.e. printed by the raster orientations of 0˚ and 45˚ as seen in Figs. 4(b) and 4(d), respectively. For the compression loading case, the sample with a raster orientation of 45˚ (Fig. 4(d)) has a higher absolute failure load (4.87 kN) than that of the sample with a raster orientation of 0˚ (4.51 kN). The sample with a raster orientation of 45˚ works better because it experiences the rupture including intralayer failure which is stronger than interlayer failure, whereas the specimen printed with a raster orientation of 0˚ experiences just buckling in its layers followed by a slight level of interlayer failure at the end of loading (see Fig. 5).

As stated earlier, in the case of samples printed by a raster orientation of 90˚(Fig. 4(e)), the amount of the failure load during tensile loading is the least (1.68 kN) compared to the cases when the raster orientation is 45˚ and 0˚. The low failure load is because the raster orientation is perpendicular to the tensile loading direction, which results in layer separation directly (i.e. interlayer failure) as seen in Fig. 3(b).

On the other hand, the failure load under compressive loading for the specimen printed by the raster orientation of 90˚ presented in Fig. 4(f) is much larger in absolute value (4.14 kN) than the load under tensile loading for the same raster orientation (1.68 kN). This result is because the layers are not

separated under compression; rather they are compressed on each other. For this reason, the absolute failure load of the sample with the raster orientation of 90˚ is close to that of the samples with raster orientations of 45˚ and 0˚ under compression. Just after huge levels of displacement (Fig. 4(f)) and experiencing large levels of plastic deformations, the sample fails by interlayer failure imposed by buckling (Fig. 3(c)).

From the failure images of PLA specimens printed by the raster orientations of 0˚ and 45˚ (Fig. 5), it can be seen that raster orientation affects the nature of the failure (i.e. either rupture or fully buckling). In both samples, first, an out-of-plane deformation (i.e. buckling) occurs. Then, for the rater orientation of 0˚ (i.e. O0C), the sample does not endure any rupture but buckling as shown in Fig. 5(a), leading to gradual interlayer failure and consequent several decreases in the load-displacement curve (see Fig. 4(b)). By contrast, for the raster orientation of 45˚, the rupture is seen along the raster orientation, indicating mainly interlayer failure as seen in Fig. 5(b). Due to the rupture, the absolute load value endures a sudden decrease after the peak load (see Fig. 4(d)).

3.2 Effect of raster orientation for PLA scarf joints

The raster orientation also influences the failure behavior of the scarf joints that includes the printed PLA adherends bonded by the adhesive in different scarf angles. To investigate the effects of raster orientation on the load-displacement responses of the scarf joint specimens of the same scarf angles, tensile test results for two raster orientations (0˚ and 45˚) are plotted together for the same scarf angle of 60˚ in Fig. 6(a) and of 15˚ in Fig. 6(b). It is seen that the scarf joints made by adherends printed with a raster orientation of 0˚ indicate lower displacements at failure and higher failure loads compared to those of the adherends printed with a raster orientation of 45˚, even though they have the same scarf angles. These similar results obtained for both scarf angles of 60˚ and 15˚, as shown in Fig. 6, reflect the consistency of the bonding because considering the results of the single PLA specimens shown in Fig. 4, it was revealed that the raster orientation of 0˚ should have a larger failure load but lower displacement at the peak load. This can be justified by the fact that intralayer failure occurs for the raster orientation of 0˚ which needs higher forces (or energy) compared to interlayer failure. As mentioned previously, one mechanism of the failure (interlayer) refers to the separation of the PLA layers from each other, due to the direction of applied loading and the orientation of the layers of PLA parts. This tendency to separation is the reason for the larger values of elongation at failure of the specimens, in which the adherends were printed with a raster orientation of 45˚ (see Fig.6).

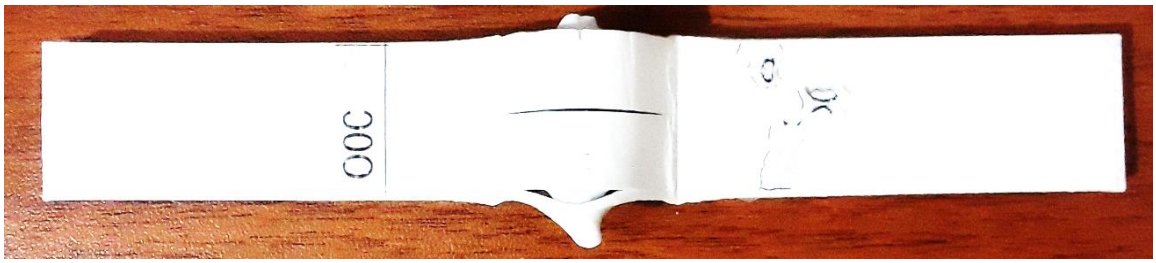

(a)

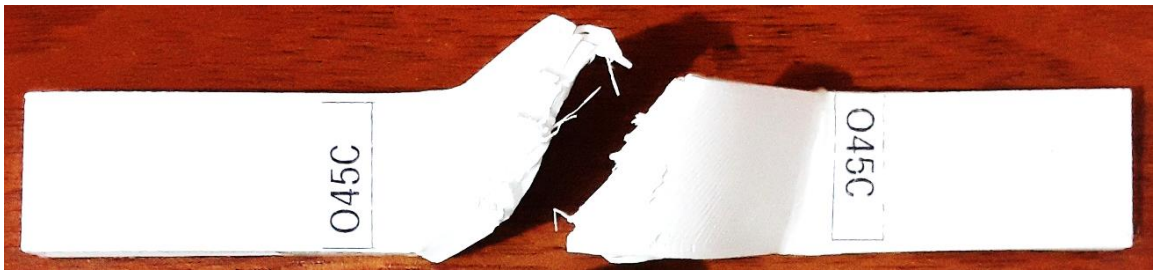

(b)

Fig.5 Failure images of single PLA specimens of different raster orientations in the compression test, (a) 0˚ raster orientation, (b) 45˚ raster orientation.

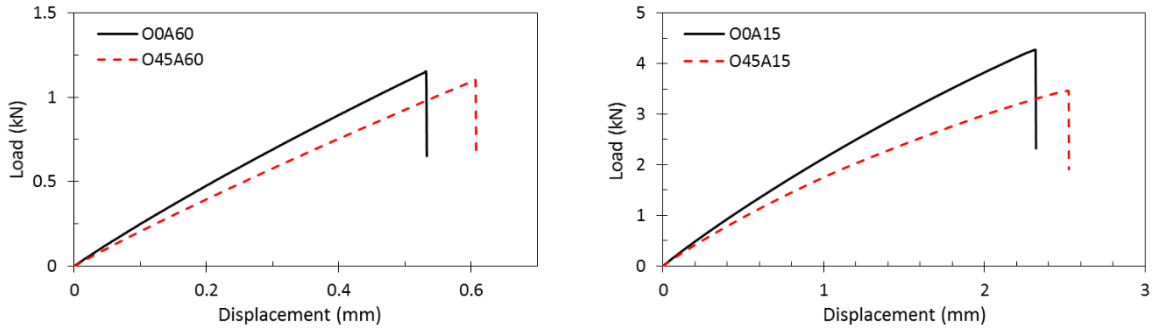

(a) (b)

Fig.6 Comparison between the tensile behaviors of the joints including adherends of different raster orientations (i.e. 0˚ and 45˚), (a) for the scarf angle of 60˚ (b) for the scarf angle of 15˚.

3.2 Effects of scarf angle for PLA scarf joints

The load-displacement results of the scarf joint specimens with different scarf angles tested in this study are shown in Fig. 7. It can be observed that for all the joints, the reduction of the scarf angles results in enhancement of the failure load and similarly in the rise of the displacement at the peak load. In addition, the behaviors of the joints were compared to those of single adherends (without any bonding), labeled as O45T and O45C in Fig. 7. The outcome has a logical trend in the change of the load-displacement curves, reflecting the fact that with reducing scarf angle the behavior is approaching to the behavior of one single PLA part without any bonding. In other words, the smaller the scarf angle, the higher the failure load, and the larger the displacement at failure.

One outlier for this behavior is the failure load of the specimen O45A45. In Fig. 7(a), as a general trend owing to a larger bondline, the sample O45A45 is supposed to have a stiffer behavior than O45A90 but due to the equivalence of the scarf angle and raster orientation of the adherends in O45A45, the joint failed sooner than expected. This is the reason for the smaller failure load and experienced displacement (elongation at failure) of O45A45 compared to the results of O45A90.

For the compressive test results in Fig. 7(b), on the other hand, there is no unusual performance with the equivalence of the scarf angle and raster orientation of the adherends. This can be justified by the fact that tensile loading causes the plates of PLA material inside the adherends to accelerate the failure of the joints under tensile loading, which is not the case for the samples under compressive loading.

Besides, there is another different behavior observed in the compressive test results in Fig. 7(b). Taking the samples O45A45 and O45A15 into account, it can be observed in Fig 7(b) that there is a limit of failure load for the scarf joints under the compressive loading because both specimens experienced the same failure load at the same displacement. However, it is worth noting that the behaviors of these joints after enduring the maximum load are different. O45A45 had a sudden drop of the load curve indicating a failure by debonding of the adhesive, whereas O45A15 had a gradual decrease of the curve indicating that it experienced some sort of buckling or slow debonding while absorbing more energy.

It is also noteworthy that the difference between the failure loads of a single adherend (O45T) and a joint with a scarf angle of 15˚ (O45A15) is less than 1 kN under tensile loading, whereas this amount is about 2.5 kN for the corresponding samples under compressive loading. Thus, based on the tensile and compressive test results in Fig. 7, it can be understood that loading type affects the load-displacement behavior completely differently, especially for the joints of smaller scarf angles (i.e. 15˚).

3.3 Joint debonding

In adhesive joints, due to the adhesive and materials used, there can be different sorts of debonding modes, e.g. adhesive, or adherend (i.e. interlayer and intralayer failures) [16]. In this study, it was observed that the debonding type was adhesive in most of the joints because the separation was observed along the surface of adhesive as in the joint O0A60 shown in Fig. 8(a). However, in a few cases such as the joint O45A15 shown in Fig. 8(b), the mechanism of the failure was changed to a combination of both adhesive and adherend (interlayer and intralayer) types. This combined type is observed when the scarf angle is low, resulting in higher failure loads. For instance, joint O45A15 has a low scarf angle of 15º and in Fig 8(b), it is seen that at the bottom the debonding occurred along the adhesive surface, which is therefore called the

adhesive debonding mode. But after some point, the failure surface is seen to be different from the adhesive surface and therefore adherent debonding occurred. The adherent is seen to be debonded along a different path of raster orientation in the middle section which is defined as an intralayer failure as seen in Fig 8(b). In the top section, on the other hand, the debonding is seen to be along the raster orientation path and therefore defined as the interlayer failure.

3.4 Optimization Study

The experimental results in this study showed that at different scarf angles the failure load can differ under tensile and compressive loadings. This difference can result in an unexpected failure of the scarf joint when a different loading condition occurs in real-life applications. To ensure the scarf joint has an acceptable behavior under both tensile and compressive loadings, an optimization study is conducted. As shown in Fig.9, optimization was done for the joints of adherends with a raster orientation of 45˚. It was done based on both the failure load and displacement at the failure of joints with three different scarf angles including 15˚, 30˚, and 45˚. The best option is the joint with a scarf angle, for which the curves corresponding to the tensile and compressive failure loads intersect each other. Considering the failure load results in Fig. 9(a), the intersection is observed at a scarf angle of about 30˚. A similar observation can be made for the displacements at maximum experienced load in Fig. 9(b). Hence, the optimized scarf angle can be selected to be 30˚. Thus, the joint O45A30 is chosen as the optimized joint.

To investigate the failure behavior of the aforementioned optimized joint, Fig. 10 indicated the rupture after tensile loading. It is seen that in the joints some of the separation occurred along the scarf angle on the adhesive layer, i.e. the adhesive failure, while the broken parts indicate that some also occurred within the PLA adherends. Hence, the transition from the adhesive failure to adherend failure is clearly seen at the scarf angle of 30˚. Thus, the failure behavior of this specimen supports the conclusion made based on Fig. 9 that the O45A30 is the optimized joint. In addition, the behavior (failure type) of the optimized joint under compression loading can be understood from Fig.3 (d).

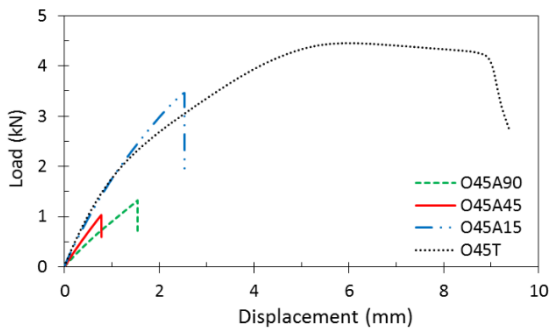

(a)

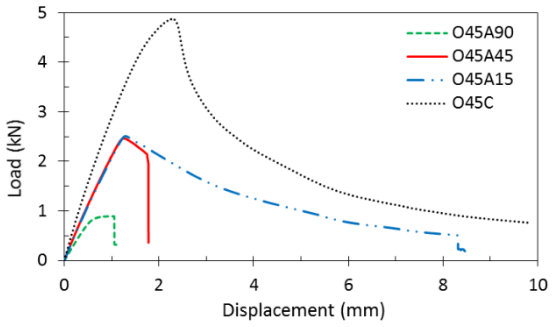

(b)

Fig.7 Comparison among the behaviors of the joints with different scarf angles (a) tensile test results (b) compressive test results. O45T and O45C show single adherends with a raster orientation of 45˚ under tensile and compression loadings, respectively. In the plot related to the compression tests (b), absolute values are given.

4. Conclusion

In this study, adhesively bonded PLA scarf joints with different scarf angles as well as 3D printed PLA parts with different raster orientations were tensile- and compressive-tested to investigate their load-displacement responses. Several raster orientations and scarf angles were utilized in the joints. The failure of the PLA scarf joints and PLA samples revealed several worthwhile results from which the remarks below can be drawn;

1. The raster orientation is a key in manufacturing PLA parts since a raster orientation of 0˚ gives the highest amounts of failure load under tensile loading while a raster orientation of 90˚ gives the lowest amount.
2. Decreasing the scarf angles results in the improvement of the joint's failure load for both the tensile and compressive loadings.
3. It was found that a scarf angle of almost 30˚ is an optimized one for the joints made of adherends with a raster orientation of 45˚, under both types of loadings.

4. The debonding mode of the joints was observed to be different depending on the scarf angle which justifies the introduced approach conducted to define the optimized joint.

Future studies can be related to the use of different adhesives (i.e. ductile and brittle types or a mixed one) and repeating the procedure of this work for those adhesives. Also, investigating the effects of complex raster orientations (e.g. +45/-45 or 0/90) and different types of adhesive joints (e.g. double-strap) on the failure behavior of the joint can be of interest.

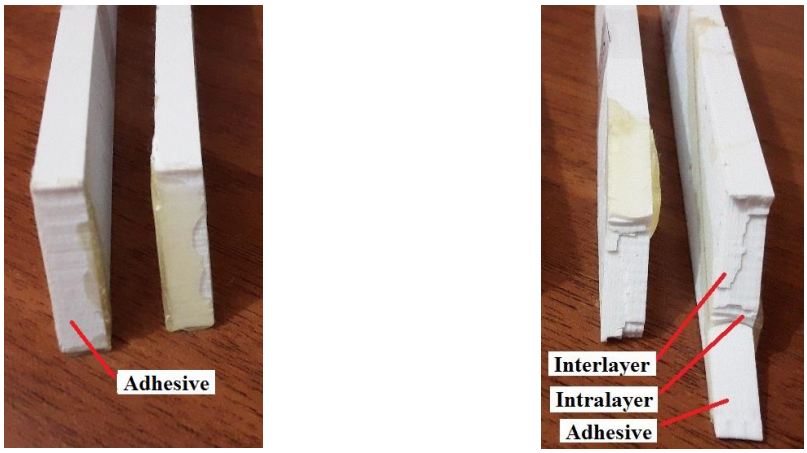

(a) (b)

Fig.8 Debonding surfaces of two selected joints, (a) O0A60, and (b) O45A15. Different types of failure including Adhesive and Adherend (Interlayer and Intralayer) were labeled in the figures.

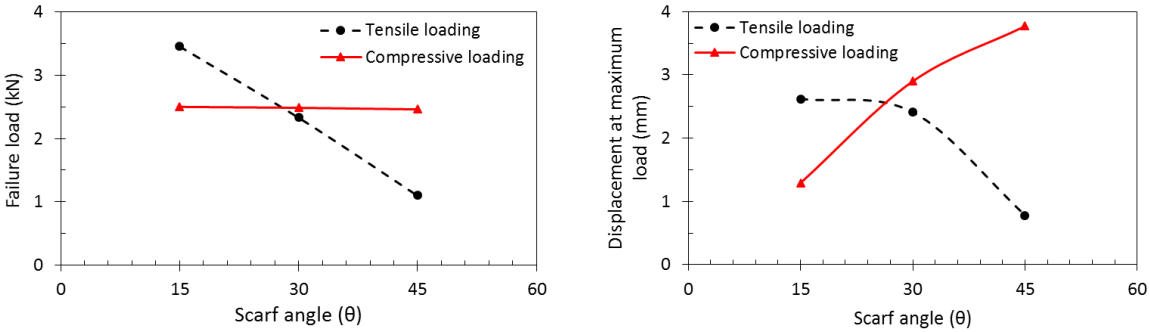

(a) (b)

Fig. 9. Optimal design for scarf joints including adherends printed with a raster orientation of 45˚ attached by Araldite 2011. Optimization based on (a) failure load of the joints, (b) displacement at the maximum experienced load by the joints, as a function of scarf angle.

Fig. 10. Demonstration of the test specimens with the optimized scarf angle of 30˚.

EKLEMELİ İMALAT İLE ÜRETİLEN PLA MALZEMELERİNİN YAPIŞTIRILMASI: YAPIŞTIRMA EĞİM AÇISININ VE BASKI YOLU YÖNELİMİNİN ETKİLERİ

Bu çalışmanın amacı, eklemeli imalat ile PLA malzemeden üretilen parçaların yapıştırıcı ile bağlanmasında, bağlantısı açısının ve baskı yolu yöneliminin etkisini araştırmaktır. İlk adımda, bütün PLA numuneleri, 0º, 45º ve 90º'lik üç farklı baskı yolu yöneliminde malzeme ekstrüzyonu eklemeli imalat yöntemi ile üretilmiştir. Bu numunelerin çekme ve basma testleri, 90º baskı yolu yöneliminin en zayıf sonuçları verdiğini göstermiştir. İkinci adımda, bütün haldeki numuneyi oluşturacak iki bağlantı parçası, 0º ve 45º baskı yolu yönelimi ile üretilmiştir. Bağlantı parçalarının yapışma bölgesi beş farklı eğim açısı ile üretilmiştir. Farklı eğim açıları ve baskı yolu yönelimlerinde oluşturulan bütün haldeki numunelerin çekme ve basma testleri, kırılma dayanımlarını belirlemek için yapılmıştır. Kırılma dayanım kuvvetinin, bağlantı parçasının baskı yolu yöneliminin ve bağlantı açısının bir fonksiyonu olarak ölçülebilir şekilde değiştiği; ancak çekme ve basma yükleri için farklı olduğu bulunmuştur. 45º baskı yolu yönelimine ve farklı eğim açılarına sahip bağlantı parçaları için bir optimizasyon çalışması yapılarak hem basma hem de çekme yükü altında kabul edilebilir bir davranışa sahip olması (kırılma kuvvetinin benzer olması) için uygun eğim açısı belirlenmiştir. Sonuç olarak uygun eğim açısının yaklaşık 30º olduğu belirlenmiştir.

REFERENCES

1. Attaran, M., *The rise of 3-D printing: The advantages of additive manufacturing over traditional manufacturing.* Business Horizons, 2017. **60**(5): p. 677-688.
2. 2. Gorguluarslan, R.M., et al., *Design and fabrication of periodic lattice-based cellular structures.* Computer-Aided Design and Applications, 2016. **13**(1): p. 50-62.
3. 3. Gorguluarslan Recep, M., et al., *An improved lattice structure design optimization framework considering additive manufacturing constraints.* Rapid Prototyping Journal, 2017. **23**(2): p. 305-319.
4. 4. Ozlati, A., et al., *An Alternative Additive Manufacturing-Based Joining Method to Make Metal/Polymer Hybrid Structures.* Journal of Manufacturing Processes, 2019. **45**: p. 217-226.
5. Frascio, M. *Joint-Design Strategies for Additive Manufacturing*. 2020.
6. Paygozar, B., S.A. Dizaji, and L.F.M. da Silva, *Bonding dissimilar materials via adhesively bonded spot-welded joints: cohesive zone model technique.* Journal of Adhesion Science and Technology, 2020: p. 1-12.
7. Kariz, M., M.K. Kuzman, and M. Sernek, *Adhesive bonding of 3D-printed ABS parts and wood.* Journal of Adhesion Science and Technology, 2017. **31**(15): p. 1683-1690.
8. Alves, D.L., et al., *Effect of material hybridization on the strength of scarf adhesive joints.* Procedia Manufacturing, 2019. **38**: p. 1244-1251.
9. Spaggiari, A. and F. Denti, *Mechanical strength of adhesively bonded joints using polymeric additive manufacturing.* Proceedings of the Institution of Mechanical Engineers, Part C: Journal of Mechanical Engineering Science, 2019: p. 0954406219850221.
10. Kioshi Kawasaki Cavalcanti, D., M. Banea, and H. Queiroz, *Mechanical Characterization of Bonded Joints Made of Additive Manufactured Adherends.* Annals of Dunarea de Jos University of Galati Fascicle XII Welding Equipment and Technology, 2019. **30**: p. 27-33.
11. Roy Choudhury, M. and K. Debnath, *Experimental analysis of tensile and compressive failure load in single-lap adhesive joint of green composites.* International Journal of Adhesion and Adhesives, 2020. **99**: p. 102557.
12. Notta-Cuvier, D., et al., *Tailoring polylactide (PLA) properties for automotive applications: Effect of addition of designed additives on main mechanical properties.* Polymer Testing, 2014. **36**: p. 1-9.
13. Kreibich, U.T. and A.F. Marcantonio, *New Developments in Structural Adhesives for the Automotive Industry.* The Journal of Adhesion, 1987. **22**(2): p. 153-165.
14. Frascio, M. and E.A.S. Marques, *Review of Tailoring Methods for Joints with Additively Manufactured Adherends and Adhesives.* 2020. **13**(18).
15. Paygozar, B., et al., *Adhesively bonded aluminium double-strap joints: effects of patch part on failure load.* Journal of the Brazilian Society of Mechanical Sciences and Engineering, 2020. **42**(11): p. 589.
16. Ghandriz, R., K. Hart, and J. Li, *Extended finite element method (XFEM) modeling of fracture in additively manufactured polymers.* Additive Manufacturing, 2020. **31**: p. 100945.